The synthesis of porous carbons from a lignin-rich residue for high-performance supercapacitors

FANG Yan-yan[1], ZHANG Qian-yu[2], ZHANG Dong-dong[2,*], CUI Li-feng[1,*]

（1. *College of Smart Energy*, *Shanghai Jiao Tong University*, *Shanghai*, 200240, *China*;
2. *Material Science and Engineering College*, *Dongguan University of Technology*, *Guangdong*, 523808, *China*）

Abstract: Fabricating electrically conductive porous electrode for supercapacitors from abundant raw materials remains a significant challenge in the field of energy storage. 3D porous carbon with high surface areas was synthesized by high-temperature carbonization and activation of lignin from cornstalks. When used as electrode materials in supercapacitors they showed a specific capacitance of 280 F g^{-1} and an area-specific capacitance of 1.3 F cm^{-2} at a current density of 0.5 A g^{-1}. An assembled symmetric supercapacitor showed a high energy density of 7.7 Wh kg^{-1} at power density of 5 200 W kg^{-1}. It is demonstrated here that the use of lignin waste to fabricate electrode materials is feasible, affording lignin new value-added utilization.

Key words: Biomass; Lignin; Hierarchical porous carbon; Supercapacitors

1 Introduction

Exploration of renewable energy sources as alternatives has aroused great concern owing to the escalating depletion of fossil fuel reserves. As a result, the use of non-gaseous emission electric vehicles has been gradually growing. Among the various electrical energy storage (EES) technologies, electrochemical capacitors (ECs) are considered to be the most important energy storage devices due to their higher power density and exceptional cyclic life as compared to batteries[1–4].

Various electrode materials such as activated carbons, metals oxides, and sulfides have been used as electrodes for ECs[5, 6]. Specifically, carbon materials have been commercialized due to their outstanding conductivity, chemical and thermal stability, and their tailor-ability in terms of structure and properties[7, 8]. More importantly, carbon materials can be obtained from a variety of natural resources. In recent years, the focus has been on developing biomass-derived carbons as electrode materials for energy storage devices[9–12]. Biomass is a renewable organic material that mainly originates from forestry and agricultural waste, which can be subsequently transformed into a myriad of high-value-added carbonaceous materials. However, it is still great challenge to achieve efficient recycling of biomass feedstocks. Among the three primary biomass feedstocks, 15%-30% lignin is the most resilient. Crucially, each structural unit is composed of the reactive hydroxyl groups, which could show pseudocapacitance in supercapacitors[13]. The carbon content of lignin is about 60% with excellent thermal stability, biodegradability, favorable renewability, and stiffness, which has been considered a promising candidate for porous carbon materials[14, 15]. Therefore, it has been demonstrated that lignin can be thermally converted into various types of carbon materials such as activated carbon[9, 10, 16], carbon fiber[17, 18], and carbon aerogel[19, 20], which could be used as electrodes for ECs. Schlee *et al*. prepared a free-standing supercapacitor electrode by direct carbonization of lignin. The as-obtained free-standing electrode delivered a gravimetric capacitance of 155 F g^{-1} with a 94% capacitance retention after 6 000 cycles[21]. Ho et al. reported a porous carbon with a surface area of 2 120 m^2 g^{-1}, and the as-assembled supercapacitor was able to deliver a capacitance of 215 F g^{-1}[22].

Received date: 2020-10-25; **Revised date:** 2021-03-18

Corresponding author: ZHANG Dong-dong, Ph. D, Lecturer. E-mail: 474177385@qq.com;
CUI Li-feng, Ph. D, Professor. E-mail: lifeng.cui@gmail.com

Author introduction: FANG Yan-yan. E-mail: fangjinzhw@163.com

Supplementary data associated with this article can be found in the online version.

In this work, a hierarchical porous carbon is prepared via scalable pyrolysis and activation of self-made lignin. Subsequently, the as-obtained activation carbon is used as the supercapacitor electrode and the electrochemical performance is evaluated. Nitrogen (N) and sulfur (S) embedded into the carbon matrix during the pyrolysis process improve the charge mobility and electrochemical performance via modifying the electronic density of carbon electrodes[23, 24]. The lignin-derived carbon (LDC) possesses a unique porous structure, which delivers high specific capacitances of 280 F g^{-1} and 1.3 F cm^{-2} at current densities of 0.5 A g^{-1}. Remarkably, the symmetric supercapacitor exhibits a high energy density of 7.7 Wh kg^{-1} with exceptional rate capability and cyclic life.

2 Experiment

2.1 Preparation of lignin

100 g of crushed corn stover of dry basis with 13.5% lignin content was added into 2.5 L of water with 20% KOH, and the mixture was heated to 120 °C in an autoclave. Subsequently, the pretreated liquor was recovered using vacuum filtration. Then hydrochloric acid was slowly added to the pretreated liquor until the pH value decreased to 2, and then it was stirred for 12 h. Later, the precipitate was collected via filtration and dried in a vacuum. Finally, the mixture was moved into a large tray and kept at 45 °C for 48 h in air and then kept at 70 °C for 24 h in air.

The obtained lignin-rich residue was carbonized at 350, 450, 550 and 650 °C with a heating rate of 5 °C min^{-1} respectively, and dwelled for 2 h under argon flow. Subsequently, the sample was cooled to room temperature. These obtained products were denoted as LDC-X (X with 350, 450, 550, 650), where X represents the pyrolysis temperature. For the activation process, 1 g of LDC was uniformly blended with 3 g of KOH using a mortar. And then the mixture was loaded onto a porcelain boat. The activation was performed at 700 °C with a heating rate of 15 °C min^{-1} and dwelled for 0.5 h in an Ar atmosphere. After the activation process, the carbon samples were washed with 5% of HCL solution and deionized water until the pH value of 7. The sample was collected and dried at 60 °C overnight.

2.2 Characterization

The morphology and microstructure of LDC were observed via scanning electron microscope (SEM) and transmission electron microscope (TEM). The N and S elements were characterized by elemental analysis and energy dispersive spectroscopy. The specifical surface area (SSA) and pore volume were evaluated based on the N_2 adsorption-desorption. X-ray photoelectron spectroscopy (XPS) and Raman spectrum were performed to measure the components of LDC.

2.3 Electrochemical measurements

All electrochemical measurements of the electrode materials were conducted using an electrochemical workstation (CHI660E). A standard three-electrode configuration was used with Hg/HgO electrode and Pt plate as the reference electrode and the counter electrode, respectively. The finely grounded LDC, carbon black, and polytetrafluoroethylene (PTFE) were mixed with a mass ratio of 8∶1∶1 to prepare the working electrode. The resultant slurry was then cast on a roller grinding machine. After that, the slurry was pressed at a pressure of 10 MPa with nickel-foam coated. The mass of the active material was approximately 4.6 mg with a thickness of 30 μm. In a two-electrode configuration test, symmetric devices (CR2032) were assembled and then measured in a BST8 cycler (MTI) at various charge-discharge rates. Electrochemical impedance spectroscopy (EIS) was performed on CHI660E. The specific capacitance (C_s) of the single electrode and (C_{cell}) device was determined from the galvanostatic charge-discharge result, using the following equations:

$$C_S = \frac{I\Delta t}{m\Delta V} \tag{1}$$

$$C_{cell} = 2\frac{I\Delta t}{m\Delta V} \tag{2}$$

The energy density was determined by

$$E = \frac{1}{2\times 3.6} C_{cell}\Delta V^2 \tag{3}$$

The power density was calculated by

$$P = \frac{E}{\Delta t}\times 3600 \tag{4}$$

where I (A) is the discharge current, and m (g) is the mass of the active materials, Δt is the discharging time. To obtain the areal capacitance (F g^{-1}), the mass loading was replaced by the area loading (g cm^{-2}). We calculated the specific capacitance (C_s, C_{cell}), energy density (E) (Wh Kg^{-1}) and power density (P) (W Kg^{-1}) based on the discharge time in the GCD curve and calculated it according to Equation (1,2).

3 Results and discussion

Fig. 1 shows the preparation process of LDC. In this regard, the prepared corn stove is used as raw materials to obtain the lignin via acid and alkali washing. And then, a pre-carbonization process was performed in 350, 450, 550, 650 °C, respectively. The target products were obtained by mixing the precursors with KOH in appropriate proportions.

The element contents of lignin and LDC are summarized in Table S1. According to the result, lignin possesses the highest elemental oxygen content of 32.20% and the lowest elemental carbon content of 61.33% and nitrogen content of 0.89%. Furthermore, the elemental carbon content in 83.03% LDC-650 is the highest among the four samples. It is shown that 0.2% sulfur and 1% nitrogen are embedded in LDC. However, there is no significant correlations between the content of sulfur and pyrolysis temperatures. The variation of nitrogen is related to the heating rate, biomass particle size and inorganic species present in the feedstock[25, 26].

As observed in the SEM image (Fig. 2a), LDC-650 exhibits an irregular and honeycomb-like porous structure with different pore sizes. TEM images of LDC-650 (Fig. 2b and c) further verify the porous structure, illustrating that the as-prepared material is composed of numerous micropores with a typical amorphous structure[27]. The EDS mappings of LDC-650 shown in Fig. 2d-f, provide the uniform distributions of N, O, and S elements across the LDC-650 matrix.

Fig. 3a-d show two characteristic peaks of the samples for Raman spectra around 1 350-1 370 cm^{-1} and 1 580-1 600 cm^{-1}, which can be assigned to defect carbon of D band and graphitic carbon of G band for LDC, respectively[28]. All spectra have been fitted into four peaks corresponding to the D*, D, D'' and G bands, respectively. The relative intensity ratio (I_D) of D band and intensity ratio (I_G) of G band were applied to evaluate the disorder and defects of LDC. Based on the calculation, the I_D/I_G of LDC-350, LDC-450, LDC-550 and LDC-650 are 0.89, 0.89, 0.90 and 0.92, respectively, indicating that LDC-350, LDC-450, LDC-650 are more disordered than LDC-550[29, 30].

The N_2 adsorption/desorption isotherm of LDC exhibits a typical type I isotherm with an obvious hysteresis loop with p/p_0 ratio of 0.4-0.85 for relative pressures, suggesting the existence of mesopores in the LDC (Fig. 4a)[6]. The adsorbed curves increase dramatically at low relative pressures, exhibiting that LDC. LDC-350, LDC-450, LDC-550 and LDC-650 have the surface areas of 2 954.22, 3 003.65, 1 524.09 and 1 228.93 m^2 g^{-1} with numerous micropores, and the corresponding pore volumes are 1.64, 1.57, 0.84 and 0.68 cm^3 g^{-1}, respectively. Furthermore, there is a shrinkage in the isotherm's knee as the pyrolysis temperature increases from 350 to 650 °C, which indic-

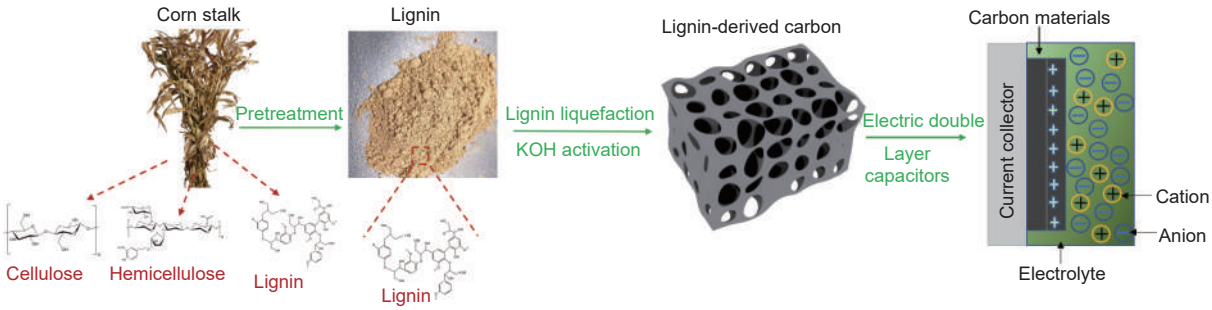

Fig. 1　Illustration of fabrication of LDC.

ates a reduction in the size of the micropore[31].

The chemical composition and surface state of LDC are analyzed by XPS. C 1s peak at 284.8 eV, O 1s peak at 532.8 eV, N 1s peak and S 2p peak are

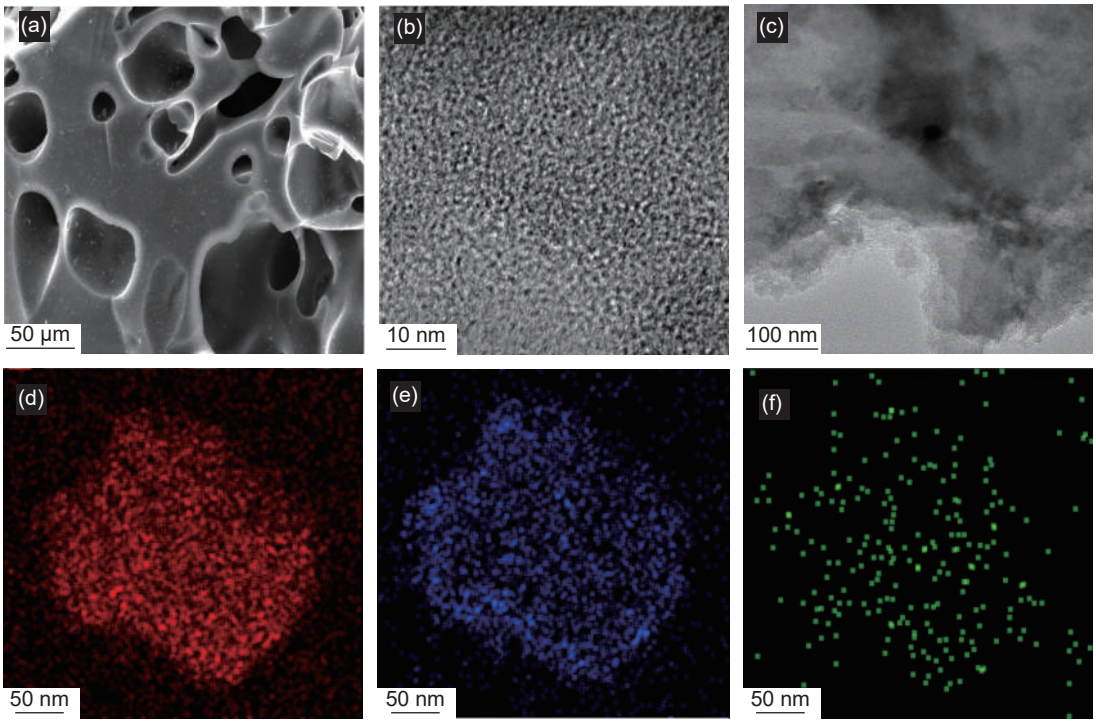

Fig. 2 (a) SEM image, (b, c) TEM images of LDC-650 and (d, e, f) EDS mappings of N, O and S.

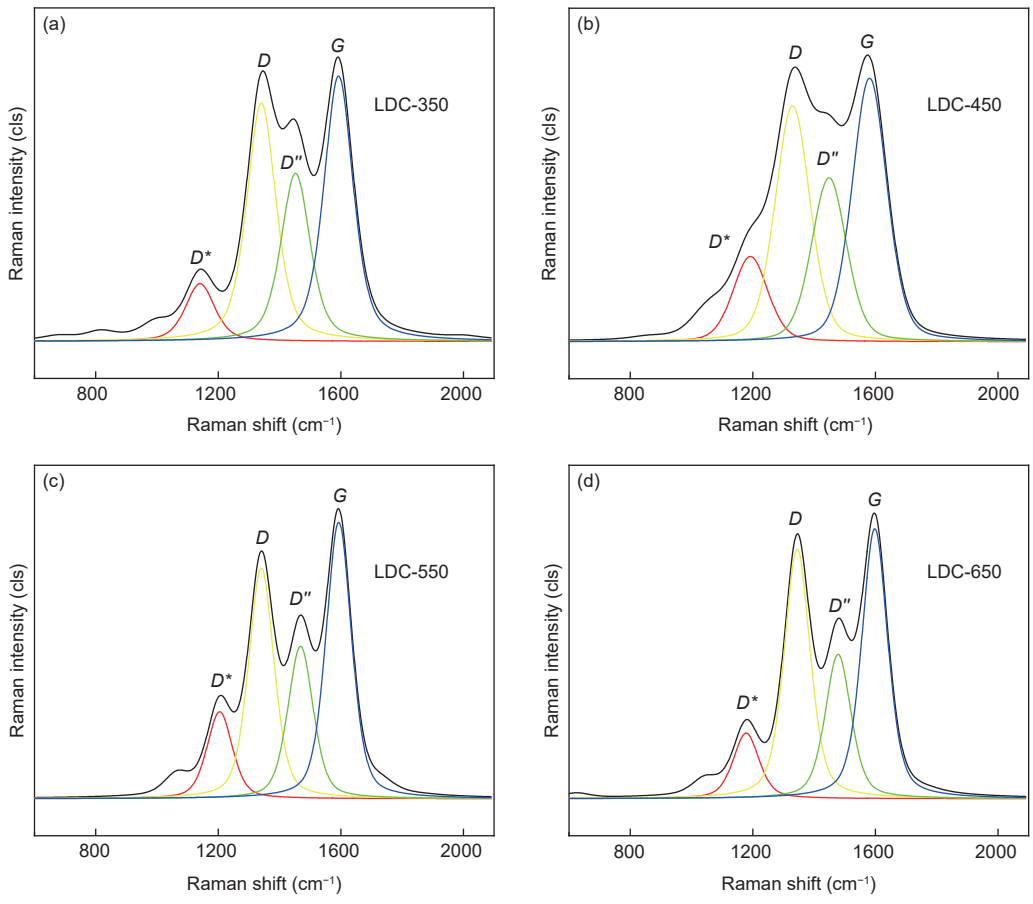

Fig. 3 Raman spectra of (a) LDC-350, (b) LDC-450, (c) LDC-550, and (d) LDC-650.

confirmed in the XPS survey spectrum of LDC (Fig. 4b), which is also shown in Table S1. As seen in Fig. 4c, the N 1s high resolution spectrum can be fitted into three peaks for 398.4, 400.1 and 401.4 eV, which could be identified as pyridinic nitrogen, pyrrolic nitrogen and graphitic nitrogen, respectively[32]. In Fig. 4d, two prominent peaks at 163.9 and 165.0 eV correspond to S $2p_{3/2}$ and S $2p_{1/2}$, which are derived from decomposing of oxidized sulfur species during the thermal treatment. The other minor peaks at 166.5 and 168.3 eV are consistent with —C—$S(O)_2$—C— sulfone bridges[33].

The potential window of the three-electrode system can be extended to 1.0 V vs. Hg/HgO. In Fig. 5a, all CV profiles of LDC exhibit a typical rectangular-like shape at scan rate of 10 mV s^{-1}, which is characteristic of a typical electric double-layer capacitor. LDC-350 exhibits a rectangular-like CV profile with the smallest area, suggesting that its capacitance is the lowest among all samples. The result could be attributed to the incomplete pyrolysis of LDC-350, which leads to its lower capacitance. The similar rectangular-like shape for the CV profiles of LDC-650 and LDC-550 implies that both samples exhibit similar specific capacitance. This result is in good agreement with their high SSA and favorable pore size distributions. The existence of nitrogen and sulfur elements in LDC can significantly enhance their wettability and introduce pseudocapacitance in the electrochemical reaction[34–36].

The resistances of LDC are measured by EIS. In a typical Nyquist plot, three main parts are present, including semicircle at high frequency, straight line with 45° slope at the middle frequency, and an almost vertical line at low frequency. As shown in Fig. 5b, LDC-350, LDC-450, LDC-550 and LDC-650 show similar first intersection of 0.5 Ω with Z' axis, which symbolizes that the internal resistance (R_s) stems from

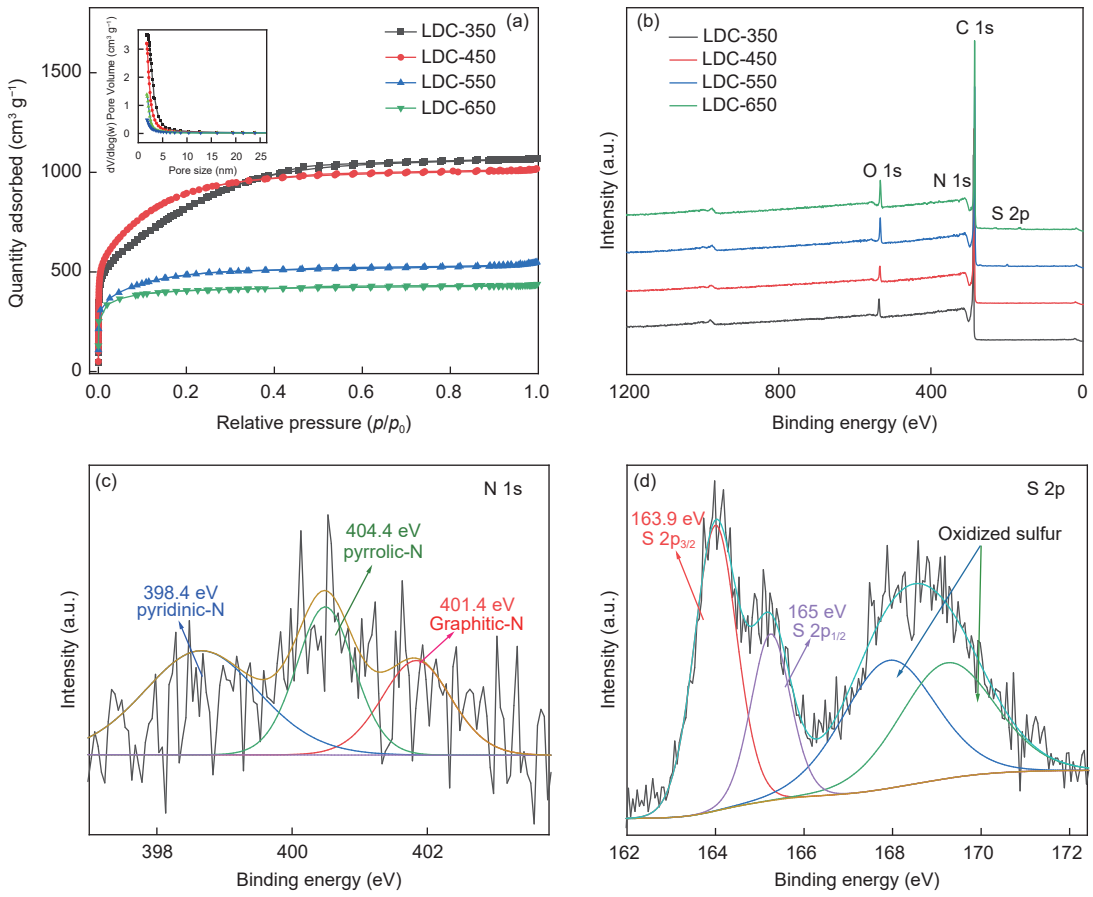

Fig. 4　(a) Nitrogen adsorption/desorption isotherms and pore sizes distribution of LDC, (b) survey XPS spectra of LDC, (c) high-resolution spectra of N 1s, and (d) high-resolution spectra of S 2p.

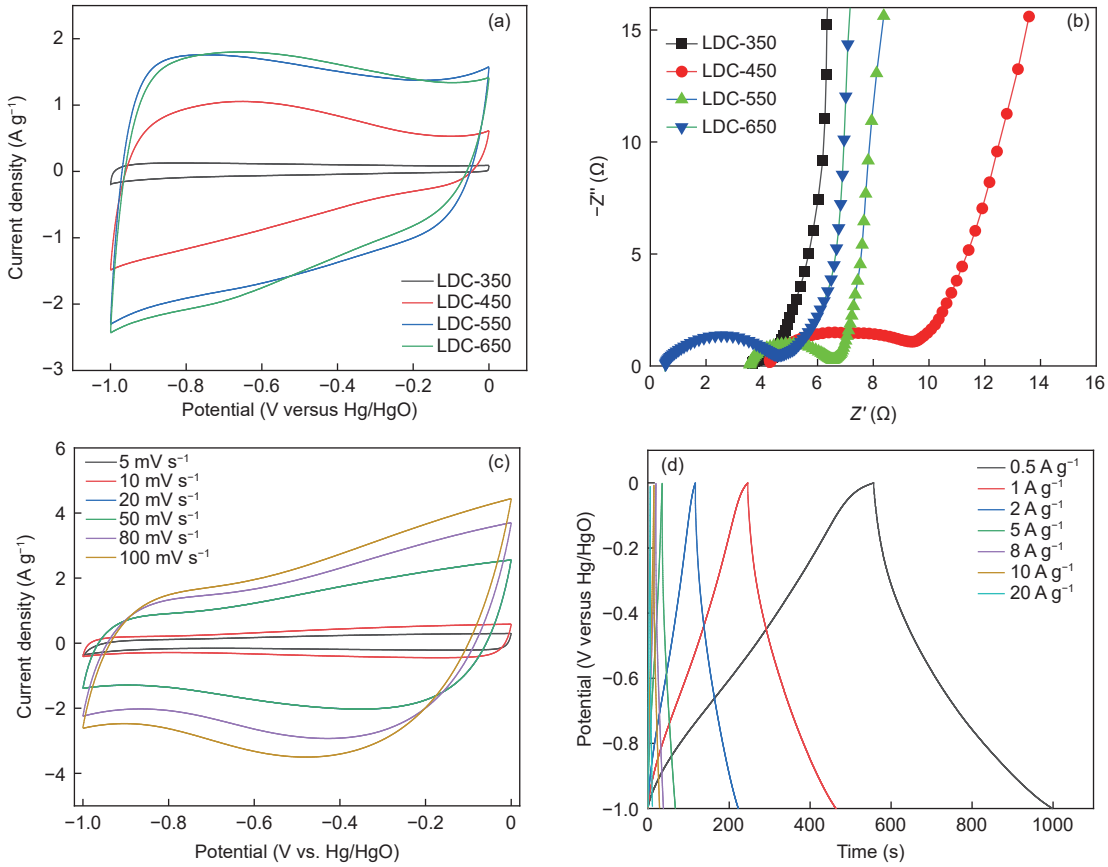

Fig. 5 (a) CV of LDC at a scan rate of 10 mV s^{-1}, (b) EIS of LDC with different pyrolytic temperatures, (c) CV of LDC-650 at various scan rates, (d) galvanostatic charge/discharge profiles of LDC-650 at various current densities.

the ionic resistance, and the contact resistance between the electrode material and current collector is identical[37]. Compared with other electrodes, LDC-350 delivers the largest semicircle, indicating the highest charge-transfer resistance (R_{ct}) at the electrode−electrolyte interface[38]. Obviously, the R_{ct} value of 0.5 Ω for LDC-650 is the lowest. In the low-frequency region, all four electrodes show nearly-vertical lines, which is typical of the supercapacitor[39].

As shown in Fig. 5c, CV was performed at the scan rates of 2, 5, 10, 20, 50, 80 and 100 mV s^{-1}, respectively. Below 50 mV s^{-1}, LDC-650 shows ideal capacitive behaviors due to nearly rectangular CV curves. With the increase of scan rates, the CV curves of LDC-650 electrode are relatively distorted, which are caused by the oxygen groups and retarded ion transport[40].

The galvanostatic charge/discharge profiles of the LDC-650 (Fig. 5d) exhibit the almost symmetric triangular shapes and have no apparent Ohmic drop at different current densities. According to Equation (1), the electrode capacitance of LDC-650 is as high as 280 F g^{-1} at 0.5 A g^{-1} with 50% capacitance retention ratio at 10 A g^{-1}, implying that LDC-650 can be applied as ideal EDLCs materials. Specially, the areal capacitance of LDC-650 is calculated to be 1.3 F cm^{-2} at 0.5 A g^{-1}. It is found that the tradeoffs between SSA, pore structure, and electrical conductivity of electrode materials play important roles in improving performance of LDC-650 [31, 41].

The property of assembled CR2032 device by LDC-650 electrode is further evaluated. The rectangular CV curves can be maintained within various scan rates from 5 to 50 mV s^{-1} (Fig. 6a). However, the CV profiles suffer from slight distortion at 80-100 mV s^{-1}, stemming from the limited ionic transportation or low mass transfer at high scan rates[42]. In Fig. 6c, it is evident that the device can retain the symmetrical triangular shapes with the increase in current densities, respectively[43].

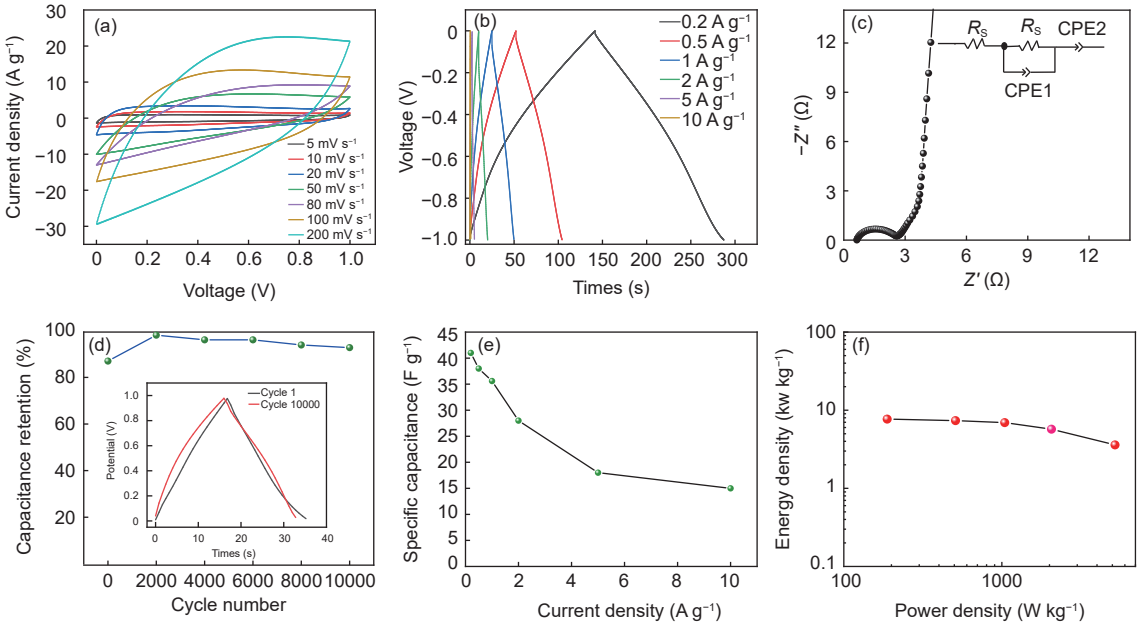

Fig. 6　(a,b) CV and GCD profiles of device, (c) nyquist plot of device, (d) cycling stability after 10 000 cycles, (e) specific capacitance at different current densities and (f) ragone plot.

To clarify the impedance of the as-assembled device, the equivalent circuit model is built based on EIS, which consists of a constant phase element (CPE), equivalent series resistance (R_s,) and charge transfer resistance (R_{ct}), as shown in Fig. 6c[44]. The fitting R_s, R_{ct} values are 0.64 and 1.9 Ω, respectively. Generally, the constant phase element originates from the surface inhomogeneity[42], specific anion adsorption[45].

The devices also exhibit a good cycling stability, with 96% capacitance retention compared with their initial capacitance (Fig. 6d). This cyclic performance by the LDC-650 devices is substantially higher than that of biomass-derived supercapacitor devices[24, 46]. As shown in Fig. 6(e), the devices still exhibit a high specific capacitance of 55 F g^{-1} at 0.2 A g^{-1} and 26 F g^{-1} at 5 A g^{-1} according to Equation (2), indicating LDC is suitable for the electrode materials of supercapacitors.

The energy density is the most crucial factor and criterion to evaluate for supercapacitors, which could be theoretically determined by voltage window and capacitance. In detail (Fig. 6f), the energy density of the devices is calculated to be 7.7 Wh kg^{-1} at a power density of 148 W kg^{-1}. Furthermore, the maximum power density is up to 5 200 W kg^{-1}. This value is higher than the commercial carbon supercapacitors. The performance of LDC-650 can be ascribed to the suitable SSA and hierarchical pore structure generated during the KOH activation. Moreover, a suitable SSA of 1 228.93 m^2 g^{-1} and PSD have the synergistic effect on enhancing the specific capacitance. The existence of heteroatoms (N, S) is also conducive to electrochemical performance due to the more site for the ions or counter ions adsorption[47].

4　Conclusions

In summary, symmetric supercapacitors were prepared using LDC as both the cathode and anode. The electrode material exhibits a large SSA, a high specific capacitance of 280 F g^{-1}, and a high areal capacitance of 1.3 F cm^{-2} at 0.5 A g^{-1}. The symmetric supercapacitor is able to yield a maximum energy density of 7.7 Wh kg^{-1} and a maximum power density of 5 200 W kg^{-1}. Meanwhile, the as-assembled supercapacitors demonstrate 96% capacitance retention after 10 000 cycles at a current density of 1 A g^{-1}. Based on these results, this work establishes a viable approach for improving the utilization of lignin waste from pulp and paper industries, and provides a new solution for the utilization of agricultural waste.

Supplementary materials

The comprehensive analysis of lignin at different pyrolysis temperatures and the summary of electrochemical data of biomass-derived carbon electrodes are available as supplementary materials.

Acknowledgment

This research was supported by National Nature Science Foundation of China (5210020050), Startup Research Fund of Dongguan University of Technology (KCYKYQD2017015 & KCYCXPT2017005 and Guangdong Basic and Applied Basic Research Foundation (Grant Nos. 2020A1515110219).

References

[1] Pandolfo A G, Hollenkamp A F. Carbon properties and their role in supercapacitors[J]. Journal of Power Sources, 2006, 157: 11-27.

[2] Frackowiak E, Abbas Q, Béguin F. Carbon/carbon supercapacitors[J]. Journal of Energy Chemistry, 2013, 22: 226-240.

[3] Simon P, Gogotsi Y. Capacitive energy storage in nanostructured carbon –electrolyte systems[J]. Accounts of chemical research, 2013, 46: 1094-1103.

[4] Yang S, Wang S, Liu X, et al. Biomass derived interconnected hierarchical micro-meso-macro porous carbon with ultrahigh capacitance for supercapacitors[J]. Carbon, 2019, 147: 540-549.

[5] Zhang L L, Zhao X S. Carbon-based materials as supercapacitor electrodes[J]. Chemical Society Reviews, 2009: 38.

[6] Li Y, Wang G, Wei T, et al. Nitrogen and sulfur co-doped porous carbon nanosheets derived from willow catkin for supercapacitors[J]. Nano Energy, 2016, 19: 165-175.

[7] Li X, Xing W, Zhuo S, et al. Preparation of capacitor's electrode from sunflower seed shell[J]. Bioresource Technology, 2011, 102: 1118-1123.

[8] Abioye A M, Ani F N. Recent development in the production of activated carbon electrodes from agricultural waste biomass for supercapacitors: A review[J]. Renewable and Sustainable Energy Reviews, 2015, 52: 1282-1293.

[9] Suhas, Carrott P J, Ribeiro Carrott M M. Lignin--from natural adsorbent to activated carbon: a review[J]. Bioresource Technology, 2007, 98: 2301-2312.

[10] Jin Y, Ruan X, Cheng X, et al. Liquefaction of lignin by polyethyleneglycol and glycerol[J]. Bioresource Technology, 2011, 102: 3581-3583.

[11] Zheng X, Lv W, Tao Y, et al. Oriented and interlinked porous carbon nanosheets with an extraordinary capacitive performance[J]. Chemistry of Materials, 2014, 26: 6896-6903.

[12] Zhu Y, Chen M, zhang Y, et al. A biomass-derived nitrogen-doped porous carbon for high-energy supercapacitor[J]. Carbon, 2018, 140: 404-412.

[13] Zhu J, Yan C, Zhang X, et al. A sustainable platform of lignin: from bioresources to materials and their applications in rechargeable batteries and supercapacitors[J]. Progress in Energy and Combustion Science, 2020: 76.

[14] Kim S K, Kim Y K, Lee H, et al. Superior pseudocapacitive behavior of confined lignin nanocrystals for renewable energy-storage materials[J]. ChemSusChem, 2014, 7: 1094-1101.

[15] Bengtsson A, Bengtsson J, Sedin M, et al. Carbon fibers from lignin-cellulose precursors: Effect of stabilization conditions[J]. ACS Sustainable Chemistry & Engineering, 2019, 7: 8440-8448.

[16] Titirici M M, White R J, Brun N, et al. Sustainable carbon materials[J]. Chem Soc Rev, 2015, 44: 250-290.

[17] Yu X, Zhang K, Tian N, et al. Biomass carbon derived from sisal fiber as anode material for lithium-ion batteries[J]. Materials Letters, 2015, 142: 193-196.

[18] Liu Y, Shi Z, Gao Y, et al. Biomass-swelling assisted synthesis of hierarchical porous carbon fibers for supercapacitor electrodes[J]. ACS Appllied Materials Interfaces, 2016, 8: 28283-28290.

[19] Hao P, Zhao Z, Tian J, et al. Hierarchical porous carbon aerogel derived from bagasse for high performance supercapacitor electrode[J]. Nanoscale, 2014, 6: 12120-12129.

[20] Cheng P, Li T, Yu H, et al. Biomass-derived carbon fiber aerogel as a binder-free electrode for high-rate supercapacitors[J]. The Journal of Physical Chemistry C, 2016, 120: 2079-2086.

[21] Schlee P, Hosseinaei O, Baker D, et al. From waste to wealth: From kraft lignin to free-standing supercapacitors[J]. Carbon, 2019, 145: 470-480.

[22] Ho H C, Nguyen N A, Meek K M, et al. A solvent-free synthesis of lignin-derived renewable carbon with tunable porosity for supercapacitor electrodes[J]. ChemSusChem, 2018, 11: 2953-2959.

[23] Yang H, Yan R, Chen H, et al. Characteristics of hemicellulose, cellulose and lignin pyrolysis[J]. Fuel, 2007, 86: 1781-1788.

[24] Zhang L, Shi G. Preparation of highly conductive graphene hydrogels for fabricating supercapacitors with high rate capability[J]. The Journal of Physical Chemistry C, 2011, 115: 17206-17212.

[25] Long C, Chen X, Jiang L, et al. Porous layer-stacking carbon derived from in-built template in biomass for high volumetric performance supercapacitors[J]. Nano Energy, 2015, 12: 141-151.

[26] Kan T, Strezov V, Evans T J. Lignocellulosic biomass pyrolysis: A review of product properties and effects of pyrolysis parameters[J]. Renewable and Sustainable Energy Reviews, 2016, 57: 1126-1140.

[27] Genovese M, Lian K. Polyoxometalate modified pine cone biochar carbon for supercapacitor electrodes[J]. Journal of Materials Chemistry A, 2017, 5: 3939-3947.

[28] Tian X, He Y, Song Y, et al. Flexible cross-linked electrospun carbon nanofiber mats derived from pitch as dual-functional materials for supercapacitors[J]. Energy & Fuels, 2020, 34: 14975-14985.

[29] Tian X, Li X, Yang T, et al. Flexible carbon nanofiber mats with improved graphitic structure as scaffolds for efficient all-solid-state supercapacitor[J]. Electrochimica Acta, 2017, 247: 1060-1071.

[30] Yang T, Song Y, Tian X, et al. Pitch-based laminated carbon formed by pressure driving at low temperature as high-capacity anodes for lithium energy storage systems[J]. Chemistry, 2020,

26: 16514-16520.

[31] Barbieri O, Hahn M, Herzog A, et al. Capacitance limits of high surface area activated carbons for double layer capacitors[J]. Carbon, 2005, 43: 1303-1310.

[32] Song Z, Duan H, Li L, et al. High-energy flexible solid-state supercapacitors based on O, N, S-tridoped carbon electrodes and a 3.5 V gel-type electrolyte[J]. Chemical Engineering Journal, 2019, 372: 1216-1225.

[33] Miao Y, Ma Y, Wang Q. Plasma-assisted simultaneous reduction and nitrogen/sulfur codoping of graphene oxide for high-performance supercapacitors[J]. ACS Sustainable Chemistry & Engineering, 2019, 7: 7597-7608.

[34] Bleda-Martínez M J, Maciá-Agulló J A, Lozano-Castelló D, et al. Role of surface chemistry on electric double layer capacitance of carbon materials[J]. Carbon, 2005, 43: 2677-2684.

[35] Okajima K, Ohta K, Sudoh M. Capacitance behavior of activated carbon fibers with oxygen-plasma treatment[J]. Electrochimica Acta, 2005, 50: 2227-2231.

[36] Ra EJ, Raymundo-Piñero E, Lee Y H, et al. High power supercapacitors using polyacrylonitrile-based carbon nanofiber paper[J]. Carbon, 2009, 47: 2984-2992.

[37] Lai L, Yang H, Wang L, et al. Preparation of supercapacitor electrodes through selection of graphene surface functionalities[J]. ACS nano, 2012, 6: 5941-5951.

[38] Qin F, Tian X, Guo Z, et al. Asphaltene-based porous carbon nanosheet as electrode for supercapacitor[J]. ACS Sustainable Chemistry & Engineering, 2018, 6: 15708-15719.

[39] Gamby J, Taberna P, Simon P, et al. Studies and characterisations of various activated carbons used for carbon/carbon supercapacitors[J]. Journal of Power Sources, 2001, 101: 109-116.

[40] He X, Li R, Qiu J, et al. Synthesis of mesoporous carbons for supercapacitors from coal tar pitch by coupling microwave-assisted KOH activation with a MgO template[J]. Carbon, 2012, 50: 4911-4921.

[41] Raymundo-Piñero E, Kierzek K, Machnikowski J, et al. Relationship between the nanoporous texture of activated carbons and their capacitance properties in different electrolytes[J]. Carbon, 2006, 44: 2498-2507.

[42] Hirschorn B, Orazem M E, Tribollet B, et al. Constant-phase-element behavior caused by resistivity distributions in films: I. Theory[J]. Journal of The Electrochemical Society, 2010, 157: C452.

[43] Xu Z, Zhang X, Li K, et al. Green synthesis of Fe-decorated carbon sphere/nanosheet derived from bamboo for high-performance supercapacitor application[J]. Energy & Fuels, 2020, 35: 827-838.

[44] Mei B A, Munteshari O, Lau J, et al. Physical interpretations of Nyquist plots for EDLC electrodes and devices[J]. The Journal of Physical Chemistry C, 2017, 122: 194-206.

[45] Pajkossy T, Wandlowski T, Kolb D M. Impedance aspects of anion adsorption on gold single crystal electrodes[J]. Journal of Electroanalytical Chemistry, 1996, 414: 209-220.

[46] Usachov D, Vilkov O, Gruneis A, et al. Nitrogen-doped graphene: Efficient growth, structure, and electronic properties[J]. Nano Lett, 2011, 11: 5401-5407.

[47] Wen Z, Wang X, Mao S, et al. Crumpled nitrogen-doped graphene nanosheets with ultrahigh pore volume for high-performance supercapacitor[J]. Advanced Materials, 2012, 24: 5610-5616.